RSC Advances

PAPER

Cite this: *RSC Adv.*, 2016, **6**, 76551

Temperature dependent Raman spectroscopy of electrochemically exfoliated few layer black phosphorus nanosheets

Amit S. Pawbake,[ab] Manisha B. Erande,[b] Sandesh R. Jadkar[b] and Dattatray J. Late*[a]

Received 20th June 2016
Accepted 3rd August 2016

DOI: 10.1039/c6ra15996f

www.rsc.org/advances

The present investigation deals with temperature dependant Raman spectroscopy of electrochemically exfoliated few layer black phosphorus nanosheets. The temperature dependent study illustrates that softening of the A_g^1, B_{2g} and A_g^2 modes occurs as the temperature increases from 78 K to 573 K. The calculated temperature coefficients for the A_g^1, B_{2g} and A_g^2 modes were found to be -0.028 cm^{-1} K^{-1}, -0.028 cm^{-1} K^{-1} and -0.018 cm^{-1} K^{-1} respectively. The observed phenomenon can be utilized for characterizing other emerging two-dimensional inorganic layered materials with atomic thickness.

Introduction

Graphene has attracted much attention due to its application in nanoelectronic and optoelectronic devices[1] due to its huge mobility of $\sim 2 \times 10^5$ cm^2 V^{-1} s^{-1} which is suitable to be used in fast communication and radio frequency devices.[2] Graphene is a promising material due to its extraordinary and unique optical,[3] electrical,[4] mechanical[5] and magnetic properties.[6] The low I_{on}/I_{off} ratio in field effect transistor devices only reinforces graphene's potential use and commercialization in various optoelectronic devices. Graphene-like two dimensional (2D) transition metal dichalcogenide (TMDC) inorganic layered materials have been widely studied recently because they are semiconducting in nature and have a tuneable bandgap, a property which is necessary to switch on and switch off devices. Recently, 2D materials[7–18] have been widely used for various applications including optoelectronics,[8] gas sensors,[9] environmental remediation,[10] solid state lubricants,[11] solar cells,[12] light emitting diodes,[13,14] field-effect transistors,[15] photodetectors[16,17] and field emitters.[18–20]

Black phosphorus (P) has several crystal structures such as orthorhombic, rhombohedral, cubic *etc.*[17] Due to its lone pair of electrons it is available in a puckered honeycomb structure instead of atomically thin flat sheets like graphene. The loan pair of electrons is one of the reasons for degradation under ambient conditions.[17,21] Black phosphorus is an elemental p-type semiconductor produced by vertical stacking of individual atomic layers; each layer is bonded by three phosphorus atoms (shown in Fig. 1a and b). Overall, black phosphorus is a stable allotrope of phosphorus under ambient conditions. Orthorhombic black phosphorus forms wrinkled layers, which are held together by weak van der Waals forces.[21] Similar to other semiconductor materials, the bandgap in bulk black phosphorus as well as in its monolayer form remains direct with a variation from 2.2 eV for monolayer to 0.3 eV for bulk which covers the entire range of the spectrum suitable for optoelectronic device applications.[21–23] An exfoliated black phosphorus flake ($\sim$10 nm thickness) based transistor has shown high mobility up to 1000 cm^2 V^{-1} s.[24,29] Black phosphorus/h-BN heterostructures have been used in solar cell applications with an efficiency of $\sim$0.05%,[25] highly stable field emitters,[26,27] field effect transistors,[28] anode materials for lithium ion batteries,[30] high performance sensors[17,31,32] *etc.*

A systematic study of the vibrational properties of electrochemically exfoliated black phosphorus nanosheets at a wide range of temperatures is still lacking in the literature. A detailed investigation of the vibrational properties of black phosphorus nanosheets is used to understand the electron–phonon interactions which can be a main limiting factor for charge carrier mobility. Thermal conductivity and heat dissipation might be some of the greatest challenges for fabricating existing silicon based electronic and optoelectronic devices. In device application, it is crucial to understand the effect of phonons due to self-heating of the device which can drastically affect the performance of the device. For manipulation of thermal conductivity and heat dissipation, it is important to investigate the electron–phonon interactions and thermodynamics of atomically thin nanosheets of black phosphorus materials synthesized using a chemical method, in order to use these nanosheets for various applications.

In this article, we report the vibrational properties of black phosphorus by means of Raman spectroscopy over a wide temperature range from 78 K to 573 K. The first order temperature coefficients (χ) associated with each Raman mode have been extracted from measured temperature dependence Raman

[a]*Physical & Materials Chemistry Division, CSIR-National Chemical Laboratory, Dr. Homi Bhabha Road, Pune 411008, India. E-mail: dj.late@gmail.com; datta099@gmail.com*

[b]*Department of Physics, Savitribai Phule Pune University, Pune 411007, India*

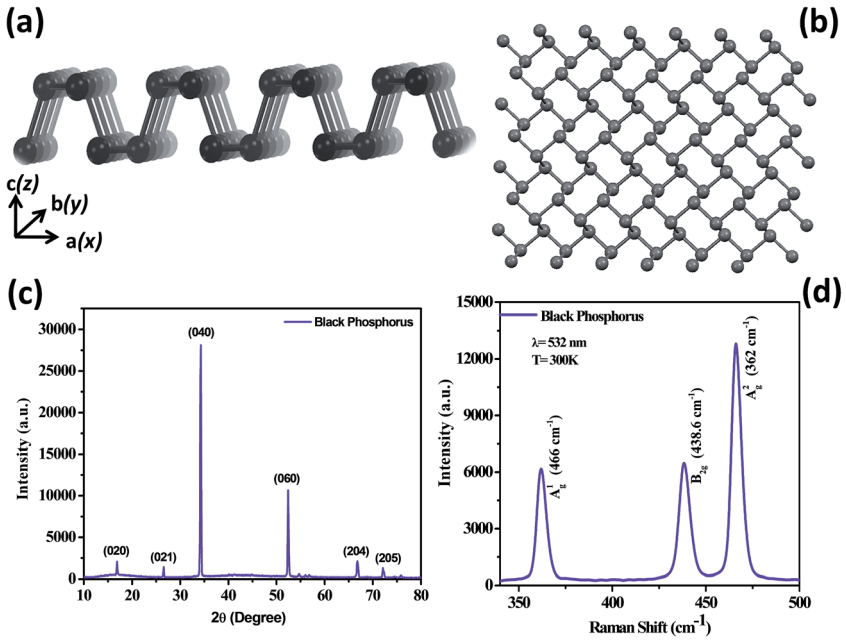

Fig. 1 Single-layer black phosphorus nanosheet: (a) side view and (b) top view, (c) typical XRD pattern of a bulk black phosphorus crystal, and (d) room temperature Raman spectrum of few layer thick black phosphorus nanosheets.

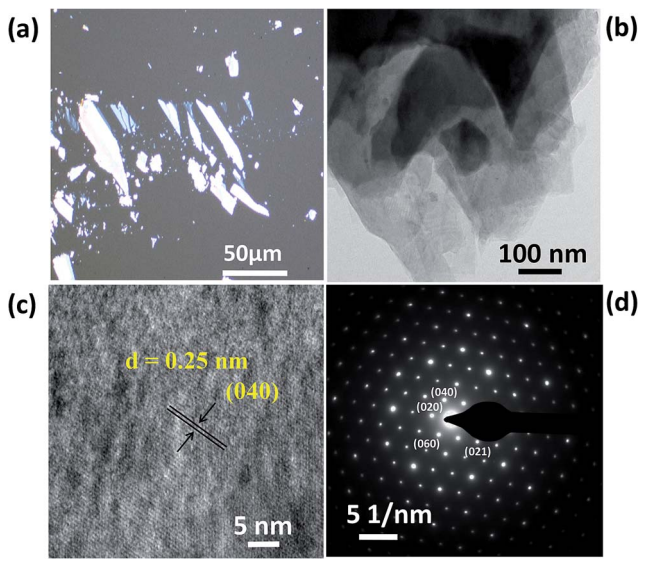

Fig. 2 Electrochemically exfoliated black phosphorus nanosheets: (a) optical image of the nanosheet sample deposited on a Si substrate, (b) typical low magnification TEM image, (c) high resolution TEM image, and (d) SAED pattern.

spectroscopy. We observe the linear nature of the temperature dependence of the Raman shifts for the A_g^1, B_{2g} and A_g^2 modes respectively.

Experimental details

The few layer thick black phosphorus nanosheets have been synthesized using electrochemical exfoliation.[26,28]

Characterization

For temperature dependant Raman spectroscopy we have used a Renishaw inVia confocal Raman microscope with a backscattering configuration. All the experiments were carried out in ambient argon with 1 mW laser power and 532 nm laser sources. Temperature dependant Raman spectroscopy was carried out over a range of 78 K to 573 K. For the low temperature measurements, we have used a liquid N_2 assembly and for high temperature we have used a heater kept below the substrate. Optical images of the electrochemically exfoliated black phosphorus nanosheet samples were captured using a Nikon Eclipse LV 150 NL microscope. For the optical images, the as-synthesized samples were dispersed in ethanol and then dropped on a Si substrate. Auto-exposure times were used during the image recording, and can be changed in the range of 10–500 ms depending upon the intensity. TEM images were captured using an FEI TECNAI G2-20 (TWIN, The Netherlands) instrument operating at 200 KV. X-Ray Diffraction (XRD) patterns for the bulk black phosphorus crystal were recorded using an X-ray diffractometer (Bruker D8 Advance, Germany) using a Cu K_α line ($\lambda = 1.54056$ Å).

Results and discussion

Fig. 1 shows a typical schematic presentation of the single-layer black phosphorus nanosheets from a (a) top view and (b) side view. Each ball represents a phosphorus atom in Fig. 1a and b. A typical XRD pattern of the bulk black phosphorus crystal shown in Fig. 1c confirms the orthorhombic crystal structure along the (040) direction. Orthorhombic black phosphorus is produced by repeated vertical stacking of individual atomic layers. The bonding of each atomic layer is oriented in multiple directions.

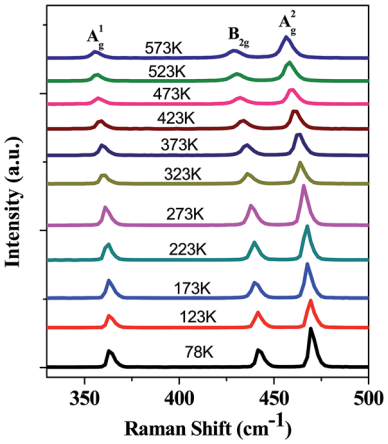

Fig. 3 Raman shift as a function of temperature for an electrochemically exfoliated few layer black phosphorus nanosheet sample.

A typical room temperature Raman spectrum of electrochemically exfoliated black phosphorus is as shown in Fig. 1d and shows high intensity A_g^1, B_{2g} and A_g^2 modes at ~466 cm^{-1}, ~438.6 cm^{-1} and ~362 cm^{-1} respectively. A typical optical image of electrochemically exfoliated black phosphorus nanosheets is shown in Fig. 2a. Further, a typical low magnification TEM image is shown in Fig. 2b, which shows a sheet-like morphology. A high resolution TEM image was also recorded which shows a *d* spacing of ~0.25 nm as depicted in Fig. 2c which shows that its orientation is along the (040) plane. Fig. 2d shows a typical indexed selected area electron diffraction (SAED) pattern of a few layer black phosphorus nanosheet sample. The diffraction pattern confirms the highly crystalline nature of the black phosphorus nanosheets. Fig. 3 shows the Raman spectrum for a few layer black phosphorus nanosheet sample as a function of temperature. The Raman spectrum shows consecutive softening of all the Raman modes with increasing temperature. The temperature dependence of the Raman modes' position is related to the electron–phonon, anharmonic phonon–phonon interactions, or pure thermal expansion. Further, an increase in the full width at half maximum (FWHM) for all the Raman modes was also observed with increasing temperature. Fig. 4a–c shows a typical plot for the Raman spectra's peak positions as a function of temperature for the A_g^1, B_{2g} and A_g^2 modes respectively. The Raman modes of the electrochemically exfoliated black phosphorus

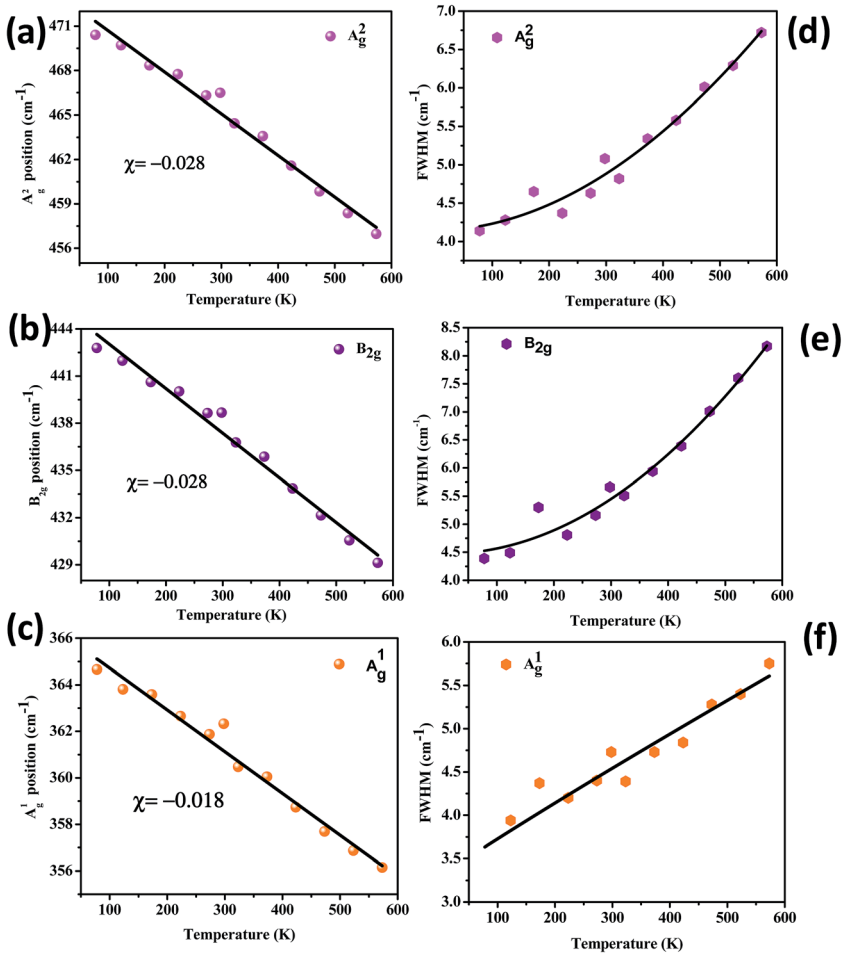

Fig. 4 Raman spectra peak position as a function of temperature for the (a) A_g^2, (b) B_{2g} and (c) A_g^1 modes respectively. The FWHM as a function of temperature for the (d) A_g^2, (e) B_{2g} and (f) A_g^1 modes showing increasing FWHM with temperature.

Table 1 Comparison of the temperature coefficients reported in the literature for various 2D nanosheets

	χ (cm^{-1} K^{-1})			
2D materials	A_g^1	B_{2g}	A_g^1	References
Black phosphorus	−0.0164	−0.0271	−0.0283	44
	−0.02175	−0.02877	−0.027	45
	−0.008	−0.013	−0.014	46
	−0.01895	−0.02434	−0.02316	45
	−0.023	−0.018	−0.023	47
	−0.028	−0.028	−0.018	Present
	χ (cm^{-1} K^{-1})			
2D materials	E_{2g}^1	A_g^1		References
MoS_2	−0.016	−0.011		34
	−0.0136	−0.0113		39
WS_2	−0.008	−0.004		34
	−0.0098	−0.014		39
	χ (cm^{-1} K^{-1})			
2D materials	A_g^1			References
$MoSe_2$	−0.0054			36
	−0.0096			39
WSe_2	−0.0071			39
	−0.0032			36

nanosheets behave linearly over the temperature range from 78 K to 573 K. The changes in the Raman frequency ($\Delta\omega$) for the A_g^2, B_{2g} and A_g^1 Raman modes of the electrochemically exfoliated black phosphorous were found to be 13.44 cm^{-1}, 13.66 cm^{-1} and 8.51 cm^{-1} respectively over the temperature range of 78 K to 573 K. The peak positions *versus* temperature were fitted using the following eqn (1),[33]

$$\omega(T) = \omega_0 + \chi T \quad (1)$$

where ω_0 is the peak position of the A_g^1, B_{2g} and A_g^2 vibration modes at zero Kelvin, χ is the first order temperature coefficient of the A_g^1, B_{2g} and A_g^2 modes. The Raman modes A_g^1, B_{2g} and A_g^2 behave linearly with temperature and the slope of the fitted straight line gives the temperature coefficient (χ). The calculated values of the temperature coefficients for A_g^1, B_{2g} and A_g^2 are found to be −0.028 cm^{-1} K^{-1}, −0.028 cm^{-1} K^{-1} and −0.018 cm^{-1} K^{-1} respectively. The observed values of the temperature coefficients are in good agreement with those reported for the TMDC;[34–39] trichalcogenide[40] and black phosphorus nanosheet[44–47] materials which are listed in Table 1. The change in the Raman frequency is given by eqn (2),[41,42]

$$\begin{aligned} \Delta\omega &= (\chi_T + \chi_V)\Delta T \\ &= \left(\frac{d\omega}{dT}\right)_V \Delta T + \left(\frac{d\omega}{dV}\right)_T \Delta V \\ \Delta\omega &= \left(\frac{d\omega}{dT}\right)_V \Delta T + \left(\frac{d\omega}{dV}\right)_T \left(\frac{d\omega}{dT}\right)_P \Delta T \end{aligned} \quad (2)$$

where $\chi = \chi_T + \chi_V$ in which χ_T is the self-energy shift due to the coupling of the phonon modes and χ_V is the shift due to the thermal expansion induced volume change. The reason these two terms arise is that all the measurements have been carried out at constant pressure rather than constant volume.[40,41]

The changes in FWHM for the A_g^1, B_{2g} and A_g^2 modes are depicted in Fig. 4d–f respectively. The broadening in the Raman modes with temperature is based on the phonon dispersion and many body theoretical calculations. The change in the FWHM is mainly due to the contribution from the decay of the zone-centre optical phonon into one acoustic and one optical phonon and these two phonons were selected from the phonon density states. The change in the line width as a function of temperature is given by the equation,[41–43]

$$\Gamma(T) = \Gamma_0 + A[1 + n(\omega_1, T) + n(\omega_2, T)] \quad (3)$$

where Γ_0 represents the background contribution, A is the anharmonic coefficient and $n(\omega, T)$ is the Bose–Einstein contribution function. The temperature dependent FWHM can be determined from the parameters such as Γ_0, A, ω_1 and ω_2. The change in the FWHM, intensity and shift in the peak position as a function of temperature can be explained by using a double resonance phenomenon which is very active in atomically thin nanosheets.

Conclusion

In summary, we have systematically performed temperature dependent Raman spectroscopy of electrochemically exfoliated black phosphorus nanosheet samples. The TEM images, and XRD and room temperature Raman spectra show the highly crystalline nature of the sample. The temperature dependent Raman spectra of few layer black phosphorous nanosheets show softening of the A_g^2, B_{2g} and A_g^1 modes. The calculated temperature coefficients for the A_g^1, B_{2g} and A_g^2 modes of the few layer black phosphorus nanosheet sample were found to be −0.028 cm^{-1} K^{-1}, −0.028 cm^{-1} K^{-1} and −0.018 cm^{-1} K^{-1} respectively. These results are explained on the basis of a double resonance phenomenon which is active in atomically thin nanosheets. Thus we realize that the A_g^1 mode is more active *via* an electron–phonon interaction. These results will be helpful in understanding the vibrational properties of atomically thin black phosphorus nanosheet based integrated circuits and useful for their thermal manipulation in the near future.

Conflict of interest

The author declares no competing financial interest.

Acknowledgements

This research work was supported by the Department of Science and Technology (Government of India) under the Ramanujan Fellowship to Dr D. J. Late (Grant No. SR/S2/RJN-130/2012), NCL-MLP project grant 028626, DST-SERB Fast-track Young scientist project Grant No. SB/FT/CS-116/2013, Board of Research in Nuclear Sciences (BRNS Grant No. 34/14/20/2015), Government of India, and partially supported by the INUP

IITB project sponsored by the DeitY, MCIT (Grant No. MT 114), Government of India.

Notes and references

1 K. S. Novoselov, D. Jiang, F. Schedin, T. J. Booth, V. V. Khotkevich, S. V. Morozov and A. K. Geim, *Proc. Natl. Acad. Sci. U. S. A.*, 2005, **102**, 10451–10453.

2 Y.-M. Lin, C. Dimitrakopoulos, K. A. Jenkins, D. B. Farmer, H.-Y. Chiu, A. Grill and P. Avouris, *Science*, 2010, **327**, 662.

3 A. N. Grigorenko, M. Polini and K. S. Novoselov, *Nat. Photonics*, 2012, **6**, 749–758.

4 S. Stankovich, D. A. Dikin, G. H. B. Dommett, K. M. Kohlhaas, E. J. Zimney, E. A. Stach, R. D. Piner, S. T. Nguyen and R. S. Ruoff, *Nature*, 2006, **442**, 282–286.

5 X. Zhao, Q. Zhang, D. Chen and P. Lu, *Macromolecules*, 2010, **43**, 2357–2363.

6 H. S. S. R. Matte, K. S. Subrahmanyam and C. N. R. Rao, *J. Phys. Chem. C*, 2009, **113**, 9982–9985.

7 H. S. S. R. Matte, A. K. Manna, D. J. Late, R. Datta, S. K. Pati and C. N. R. Rao, *Angew. Chem., Int. Ed.*, 2010, **122**, 4153–4156.

8 Q. H. Wang, K. Kalantar-Zadeh, A. Kis, J. N. Coleman and M. S. Strano, *Nat. Nanotechnol.*, 2012, **7**, 699–712.

9 D. J. Late, Y.-K. Huang, B. Liu, J. Acharya, S. N. Shirodkar, J. Luo, A. Yan, D. Charles, U. V. Waghmare, V. P. Dravid and C. N. R. Rao, *ACS Nano*, 2013, **7**, 4879–4891.

10 P. F. Weck, E. Kim and K. R. Czerwinski, *Dalton Trans.*, 2013, **42**, 15288–15295.

11 A. N. Enyashin, L. Yadgarov, L. Houben, I. Popov, M. Weidenbach, R. Tenne, M. Bar-Sadan and G. Seifert, *J. Phys. Chem. C*, 2011, **115**, 24586–24591.

12 J. Dai and X. C. Zeng, *J. Phys. Chem. Lett.*, 2014, **5**, 1289–1293.

13 G. L. Frey, K. J. Reynolds, R. H. Friend, H. Cohen and Y. Feldman, *J. Am. Chem. Soc.*, 2003, **125**, 5998–6007.

14 F. Xia, H. Wang, D. Xiao and M. Dubey, *Nat. Photonics*, 2014, **8**, 899–907.

15 D. J. Late, B. Liu, H. S. S. R. Matte, V. P. Dravid and C. N. R. Rao, *ACS Nano*, 2012, **6**, 5635–5641.

16 A. S. Pawbake, R. G. Waykar, D. J. Late and S. R. Jadkar, *ACS Appl. Mater. Interfaces*, 2016, **8**, 3359–3365.

17 M. Buscema, D. J. Groenendijk, S. I. Blanter, G. A. Steele, H. S. J. van der Zant and A. Castellanos-Gomez, *Nano Lett.*, 2014, **14**, 3347–3352.

18 C. S. Rout, P. D. Joshi, R. V. Kashid, D. S. Joag, M. A. More, A. J. Simbeck, M. Washington, S. K. Nayak and D. J. Late, *Sci. Rep.*, 2013, **3**, 3282.

19 S. R. Suryawanshi, A. S. Pawbake, M. S. Pawar, S. R. Jadkar, M. A. More and D. J. Late, *Mater. Res. Express*, 2016, **3**, 035003.

20 D. J. Late, P. A. Shaikh, R. Khare, R. V. Kashid, M. Chaudhary, M. A. More and S. B. Ogale, *ACS Appl. Mater. Interfaces*, 2014, **6**, 15881–15888.

21 A. Castellanos-Gomez, *J. Phys. Chem. Lett.*, 2015, **6**, 4280–4291.

22 A. Yuichi, S. Endo and S. Narita, *J. Phys. Soc. Jpn.*, 1983, **52**, 2148–2155.

23 R. W. Keyes, *Phys. Rev.*, 1953, **92**, 580.

24 F. Xia, H. Wang and Y. Jia, *Nat. Commun.*, 2014, **5**, 4458.

25 M. Buscema, D. J. Groenendijk, G. A. Steele, H. S. J. van der Zant and A. Castellanos-Gomez, *Nat. Commun.*, 2014, **5**, 4651.

26 M. B. Erande, S. R. Suryawanshi, M. A. More and D. J. Late, *Eur. J. Inorg. Chem.*, 2015, 3102–3107.

27 S. R. Suryawanshi, M. A. More and D. J. Late, *J. Vac. Sci. Technol., B*, 2016, **34**, 041803.

28 M. B. Erande, M. S. Pawar and D. J. Late, *ACS Appl. Mater. Interfaces*, 2016, **8**, 11548–11556.

29 L. Li, Y. Yu, G. J. Ye, Q. Ge, X. Ou, H. Wu, D. Feng, X. H. Chen and Y. Zhang, *Nat. Nanotechnol.*, 2014, **9**, 372–377.

30 C. M. Park and H. J. Sohn, *Adv. Mater.*, 2007, **19**, 2465–2468.

31 A. N. Abbas, B. Liu, L. Chen, Y. Ma, S. Cong, N. Aroonyadet, M. Kopf, T. Nilges and C. Zhou, *ACS Nano*, 2015, **9**, 5618–5624.

32 D. J. Late, *Microporous Mesoporous Mater.*, 2016, **225**, 494–503.

33 E. S. Zouboulis and M. Grimsditch, *Phys. Rev. B: Condens. Matter Mater. Phys.*, 1991, **43**, 12490.

34 M. Thripuranthaka, R. V. Kashid, C. S. Rout and D. J. Late, *Appl. Phys. Lett.*, 2014, **104**, 081911.

35 D. J. Late, U. Maitra, L. S. Panchakarla, U. V. Waghmare and C. N. R. Rao, *J. Phys.: Condens. Matter*, 2011, **23**, 055303.

36 D. J. Late, S. N. Shirodkar, U. V. Waghmare, V. P. Dravid and C. N. R. Rao, *ChemPhysChem*, 2014, **15**, 1592–1598.

37 M. Thripuranthaka and D. J. Late, *ACS Appl. Mater. Interfaces*, 2014, **6**, 1158–1163.

38 D. J. Late, *ACS Appl. Mater. Interfaces*, 2015, **7**, 5857–5862.

39 A. Pawbake, M. Pawar, S. R. Jadkar and D. J. Late, *Nanoscale*, 2016, **8**, 3008–3018.

40 A. S. Pawbake, J. O. Island, E. Flores, J. R. Ares, C. Sanchez, I. J. Ferrer, S. R. Jadkar, H. S. J. van der Zant, A. Castellanos-Gomez and D. J. Late, *ACS Appl. Mater. Interfaces*, 2015, **7**, 24185–24190.

41 P. H. Tan, Y. M. Deng and Q. Zhao, *Phys. Rev. B: Condens. Matter Mater. Phys.*, 1998, **58**, 5435.

42 P. H. Tan, Y. M. Deng, Q. Zhao and W. C. Cheng, *Appl. Phys. Lett.*, 1999, **74**, 1818.

43 J. Menendez and M. Cardona, *Phys. Rev. B: Condens. Matter Mater. Phys.*, 1984, **29**, 2051.

44 A. Lapinska, A. Taube, J. Judek and M. Zdrojek, *J. Phys. Chem. C*, 2016, **120**, 5265–5270.

45 Z. Luo, J. Maassen, Y. Deng, Y. Du, R. P. Garrelts, M. S. Lundstrom, P. D. Ye and X. Xu, *Nat. Commun.*, 2015, **6**, 8572.

46 D. J. Late, *ACS Appl. Mater. Interfaces*, 2015, **7**, 5857–5862.

47 S. Zhang, J. Yang, R. Xu, F. Wang, W. Li, M. Ghufran, Y. W. Zhang, Z. Yu, G. Zhang, Q. Qin and Y. Lu, *ACS Nano*, 2014, **8**, 9590–9596.